Nano Structured Perovskite-type Oxides with Rare Earth for Semiconductive Gas Sensor

Masami MORI*, Hiromichi AONO*, Yoshiteru ITAGAKI*, and Yoshihiko SADAOKA*

Finer perovskite-type $SmFe_{1-x}Co_xO_3$ oxides formed by the thermal decomposition of the corresponding heteronuclear hexacyano complexes. With an increase in the treatment temperature, the particle size increased from 20nm (350°C) to 400nm (1000°C). For $SmFeO_3$ prepared by the pyrolysis of the complex at 900°C, the sensing characteristics were examined for O_3, NO_2, MEK, EtOH and C_6H_6. The conductance was responsible to sub-ppm level's ozone and the sensitivity decreased with an increase in the working temperature. The sensitivity to 0.1ppm ozone was ca.1000 at 250°C. The partial replacing of Fe with Co resulted an increase in the conductance and the sensitivity to ozone decreased with an increase in the Co content, i.e., the sensitivity of $SmFe_{0.90}Co_{0.10}O_3$ at 100°C for 0.4ppm ozone was 200.

Key Words: Heteronuclear complex, Thermal decomposition, Perovskite material, Gas sensor, Ozone, NO_2, VOC

1. Introduction

Recently, renewed interests in the perovskite-type oxides with rare earth ions are given by their functional properties such as mixed conductivity by both ion and electron migration and highly nonstoichiometric composition, which permit their use in many innovative technological applications. These materials are active oxidation catalysts [1], and it can be employed as cathodes and membranes in solid oxide fuel cells [2], as electrode materials [3,4], and active materials for chemical sensors [5-9]. For these applications, the preparation of powders with controlled stoichiometry and microstructure is demanded to achieve either dense or porous structures. The conventional method of heterometallic oxide production (solid-state reaction at high temperatures of the corresponding single oxides mixture) have several problems such as a crystal growth, the change of the atomic stoichiometric ratio, and ease for the second phase formation. This solid-state reaction method does not allow a close control of powder quality and to get finer particles.

It is well known that chemical processing methods permits to lower the synthesis temperature and to improve homogeneity and reproducibility of the ceramic products [10]. Gallagher firstly proposed the formation of $LnFeO_3$ and $LnCoO_3$ from the corresponding hexacyano-complexes in 1968 [11]. These complexes can be prepared from the reactions, $LnX_3(aq) + K_3T(CN)_6(aq) \rightarrow LnT(CN)_6 \cdot nH_2O(s) + 3KX(aq)$, (T=Fe, Co, X=Cl, NO_3). The resulting products are stoichiometric within the accuracy of the chemical analysis [12]. It seems that this method is very useful to obtain perovskite-type oxides at low temperatures. The formation of perovskite-type oxide is depended on only a decomposition process at low temperature and is not necessary the solid diffusion process at high temperature as oxides mixtures, because the complexes as the precursors possess the desired stoichiometry of the rare-earth ferri- or cobalti-cyanides in a single compound.

Our aim is to develop the oxidative gas sensor using finer rare-earth perovskite-type oxides having oxidative catalytic activity and semiconducting behavior. The results of the characterizations of the complexes and the thermal decomposed products in the series $Sm[Fe_yCo_{1-y}(CN)_6] \cdot nH_2O$, and the application to chemical sensors of NO_2 and O_3 in air contaminated with and without VOCs are reviewed. [13-30].

*愛媛大学大学院理工学研究科物質生命工学専攻

Materials Science and Biotechnology, Graduate School of Science and Engineering, Ehime University

平成 18 年 11 月 1 日 受付 , 平成 19 年 1 月 31 日 受理

2. Experimentals

2-1. Structural Characterization of the Complexes

The XRD patterns of $Ln[Fe(CN)_6]\cdot nH_2O$ suggested the orthorhombic structures and the crystal parameters were determined. Linear relationships between lattice parameters and the radii, r_s, of Ln ion (Shannon's crystal radius) were confirmed. The correlation between the lattice parameters of $Ln'_xLn''_{1-x}[Co(CN)_6]\cdot 4H_2O$ and the radii of the Ln ions was examined. Here, we have the effective radius parameter of the rare earth ions in the complexes, defined as $r_{eff} = x\ r_{Ln'} + (1-x)\ r_{Ln'}$. Linear relationships between the lattice parameters and r_{eff} were also observed. These observed results suggest that the $LnFe_XCo_{1-X}$-complexes are not a mixture of powders of each LnFe- and LnCo-complex.

2-2. Thermal Decomposition of the Complexes

TGA curve of the complexes, with a heating rate of 5°C/min in syn-air was examined. The dehydration of complexes started at about 50°C and the plateau was observed in the temperature range of 240 to 300°C. The weight loss percentage at 280°C was in good agreement with the value calculated by assuming the dehydration of 4 water molecules. Further heating caused an abrupt weight loss by the decomposition of cyanide group (exothermal decomposition begins at ~350°C and a gradual decreases were observed to ~720°C, followed by the last plateau.

For the LnFe- and LnCo-complex heated at 400°C in air, FT-IR absorption bands attributable to CO_3 and NO_3 were observed in the 1300-1500 cm^{-1} region. The carbonates and nitrate gradually decomposed with an increase in the heat-treatment temperature (>620°C) for the both complexes. Similar results were also observed for $LnFe_xCo_{1-x}$-complexes. For examined complexes decomposed at 800°C, the carbonate and nitrate signals were no longer detected.

The XRD profiles of the LnFe- and LnCo-complexes decomposed at 800°C are shown in **Figs.1** and **2**, respectively. In the case of the LnFe-complexes, for Ln=Pr through Gd, only the peaks due to the perovskite-type oxide were observed, while for Ln=Dy through Yb a single phase of the perovskite-type oxide could not be obtained. Therefore, we evaluated the lattice parameters of the LnFe-complex decomposed at 800°C for Ln=Pr through Gd assuming as a reference the orthorhombic structure of $SmFeO_3$ (JCPDS file No. 39-1490, orthorhombic). For the LnCo-complexes, a single phase of perovskite-type oxide was observed for Ln = Pr through Gd, while Ln_2O_3

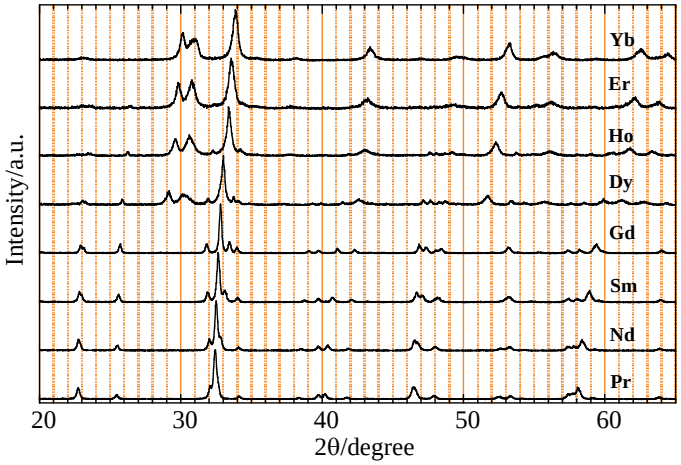

Fig. 1. XRD results for LnFe-complexes decomposed at 800 °C. Ln species are shown in the figure.

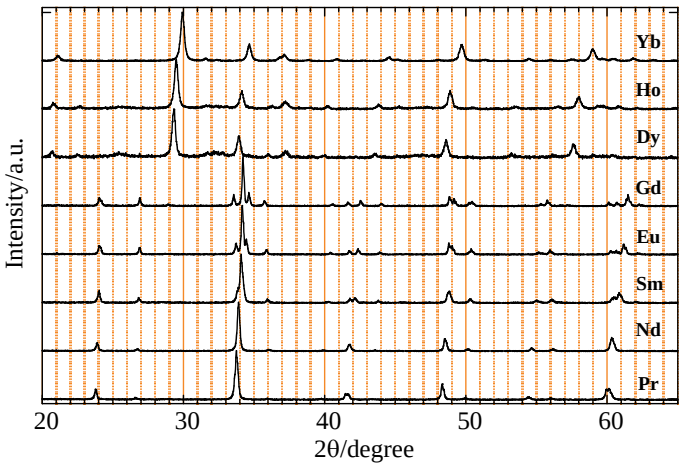

Fig. 2. XRD results of LnCo-complexes decomposed at 800 °C. Ln species are shown in the figure.

was detected as a main product for Ln = Dy through Yb. The oxides decomposed at 800°C is classified two groups by the Ln ion for both the T=Fe and Co systems.

(1) Ln=Pr~Gd Perovskite-type single phase

(2) Ln=Dy~Yb Mixture of oxides

XRD profiles of the $LnFe_XCo_{1-X}$-complexes decomposed at 800°C were also examined. The XRD profiles of the decomposed $LnFe_XCo_{1-X}$-complexes almost agree with the those of LnFe- and LnCo-perovskite-type oxides, whereas the positions of the detected signals are situated between the corresponding positions observed for LnFe- and LnCo-perovskite-type oxides for Ln=Pr through Gd. The estimated lattice parameters are shown in **Fig.3**. These observed results clearly showed that the decomposed $LnFe_XCo_{1-X}$-complex was not a mixture of powders of each LnFe- and LnCo-perovskite-type oxide. The lattice parameters, a-, b- and c-lattice parameters (crystal system; orthorhombic) increased linearly with the ratio of Fe/Co for the perovskite-type oxide. For Ln=Dy through Lu, Ln_2O_3 phase was observed as a majority product for x=0, its content decreased with an increase in the Fe content, however a single phase of the perovskite-type oxide could not be formed for x=1. The perovskite-type oxide for the Fe-system would be more easy to form compared with the Co-system.

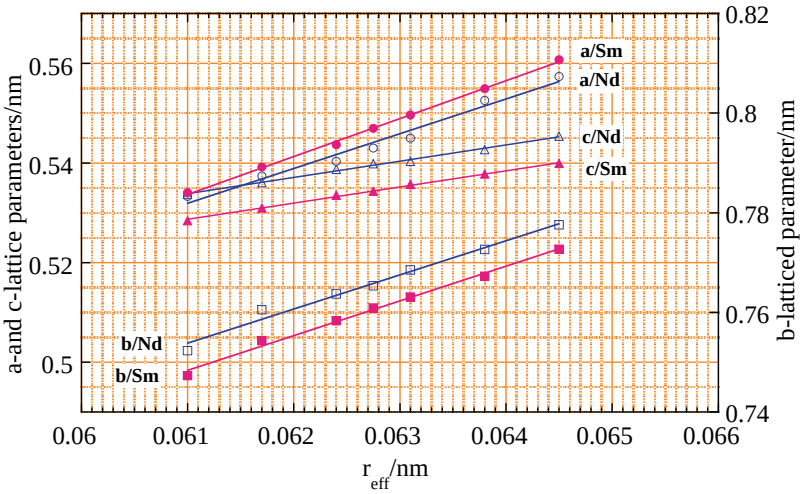

Fig. 3. The correlation between the lattice parameters and ionic radius (C.N.6) of T^{3+} for $LnFe_XCo_{1-X}$-complexes (Ln=Nd and Sm) decomposed at 800 °C.

For the complex decomposed at 350 °C for 1 hr, the XRD pattern showed some peaks attributed to perovskite-type $LaFeO_3$, together with a broad band centered at about 30° in 2θ and the signals due to the single oxides were not observed. The intensity of the broad band weakened with increasing the holding time and almost disappeared when the holding time reached 100 hrs. The XRD profile of a 1:1 mixture of La_2O_3 and Fe_2O_3 heat-treated at 600°C was also examined for comparison. For the mixture heat-treated at 600°C, all the signals were attributed to La_2O_3 and Fe_2O_3 without $LaFeO_3$. The specific surface area for the complex decomposed at 350°C changed with the holding time. With the holding time, the specific surface area decreased from 45 m^2g^{-1} to 25 m^2g^{-1} and then increased up to 38 m^2g^{-1} (the mean particle diameter is about 23 nm for density 6.67). **Figure 4-1** shows the TEM micrographs of the complex decomposed at 350°C. For the complex decomposed at 350°C for 1 hr, the formations of finer particles were detected, the SADP in this case showed the formation of polycrystalline, orthorhombic $LaFeO_3$ phase and the particle size was estimated in the order of 30 nm. The particle size of the sample decomposed for 66 hrs was slightly smaller than that of the sample decomposed for 1 hr. The increase in the specific surface area is related to the decomposition of the

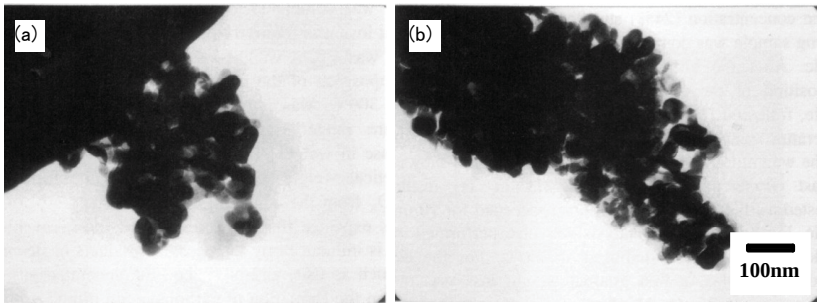

Fig. 4-1. TEM photographs of LaFe complex decomposed at 350°C for 1 (a) and 66 h (b).

intermediate compounds, such as carbonate and nitrates formed on the particle surfaces. It seems that these intermediates facilitate the formation of the nano-sized $LaFeO_3$ powders. The particle size increased with the temperature as shown **in Fig.4-2**.

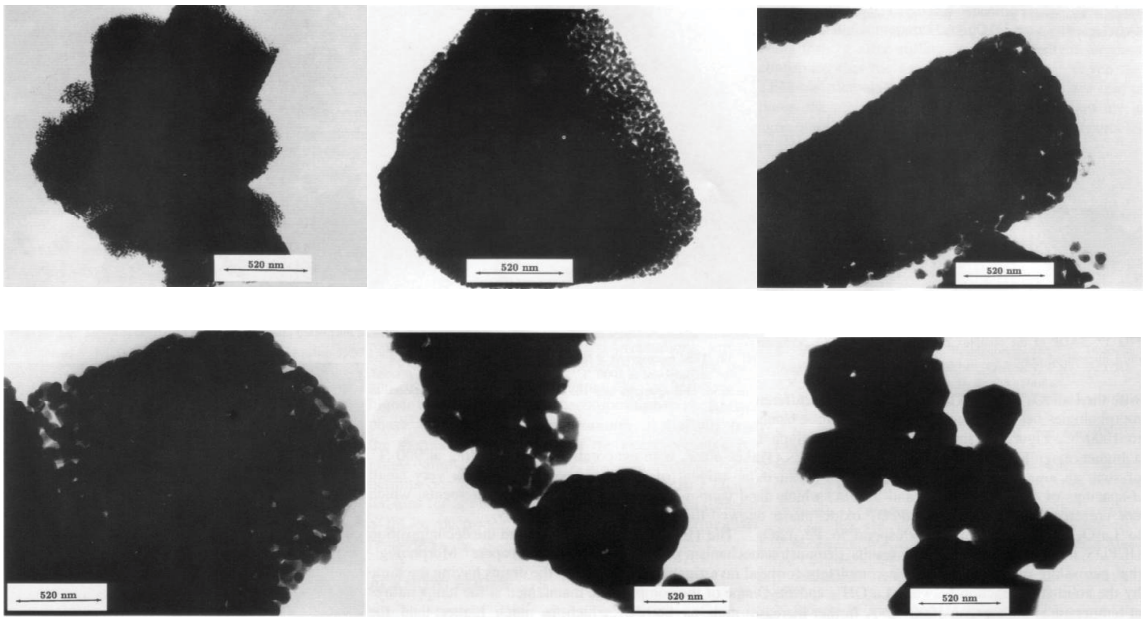

Fig.4-2. TEM photographs of the LaFe-complex decomposed at, 500(a), 600(b), 700(c), 800(d), 900(e) and 1000oC (f).

2-3. Characterization of the surface of $LnFeO_3$

The surface of the particles was examined by XPS for $LnFeO_3$ (Ln=La, Nd, Sm, Gd, and Dy). The O_{1s} peaks could be classified to two components. The first one at a lower BE that can be ascribed to oxygen ($O^{2-}_{lattice}$) in the lattice of the perovskite-type structure, and the second component at a higher BE that is ascribed to surface adsorbed oxygen (O^{-}_{ad}). In **Table 1**, the elemental ratios on the surface (within 3 or 4 layers from the top of the surface; depth detectable by XPS) are summarized. The Ln/(Ln+Fe) ratio was larger than 0.5 for the $LnFeO_3$ powders examined. The $O_{lattice}$/(Ln+Fe) ratio was around 1.5 and the lowest value, 1.3, was confirmed for Ln=Sm. The highest O_{ad}/(Ln+Fe) ratio, 1.24, was also confirmed for Ln=Sm.

Table 1. Elemental ratios determined by XPS.

Sample	Ln/(Ln+Fe)	$O_{lattice}$/(Ln+Fe)	O_{ad} /(Ln+Fe)	(O_{ad}+$O_{lattice}$)/(Ln+Fe)
$LaFeO_3$	0.544	1.596	0.699	2.293
$NdFeO_3$	0.579	1.415	0.743	2.158
$SmFeO_3$	0.655	1.300	1.237	2.537
$GdFeO_3$	0.611	1.527	0.870	2.397
$DyFeO_3$	0.602	1.486	0.823	2.309

For the powders pre-heated in N_2 and air atmosphere at 800°C for 1 hr, the XPS analysis was applied in a high vacuum and the estimated surface characteristics for oxygen content are summarized in **Table 2**. The ratio of [O_{ad}]/[$O_{lattice}$] was influenced by the heat-treatment conditions. For the sample heated at 700°C which was same temperature of the thermal decomposition of the complex, the value of [O_{ad}]/[$O_{lattice}$] ratio was about 0.6 which was hardly influenced by the heat-treatment ambient. The [O_{ad}]/[$O_{lattice}$] ratio of the surface for the powders heated in nitrogen at 800°C and 900°C

showed higher value than those heat-treated in air. These differences suggested that the total number of the sites for oxygen adsorption was is influenced by the ambient and the temperature. For the sample heated in air, the ratio of $[O_{lattice}]/[La+Fe]$ was around 1.5 corresponding to the chemical formula of $LaFeO_3$. The results suggested that the lattice oxygen vacancies were poorly formed on the surface when the samples were heat-treated in air. It is concluded that the increase in the weight in air above 650°C would be attributable to be formation of lattice oxygen ($O_{lattice}$). The decrease in weight above 900°C is due to the lack of the lattice oxygen. On the other hand, the $[O_{lattice}]/[La+Fe]$ ratio decreased to ca. 1.1 for the samples heated in nitrogen above 800°C. The gradual decrease in the weight observed for the powders heating in nitrogen would be attributable to the formation of the oxygen vacancies (change from the lattice oxygen to the adsorbed oxygen). The total oxygen ratio of $[O_{lattice}+O_{ad}]/ [La+Fe]$ was about 2.2 which was hardly influenced by the heat-treatment process and ambient. It was concluded that the heat-treatment in nitrogen at 800-900°C was effective to increase the adsorption sites of oxygen without structural deformations of the body.

Table 2. Elemental ratios determined by XPS.

Temp./°C	ambient	$[O_l]/[La+Fe]$	$[O_{ad}]/[La+Fe]$	$[O_l+O_a]/[La+Fe]$	$[O_{ad}]/ [O_l]$
700	Air	1.54	0.87	2.41	0.56
800	Air	1.61	0.45	2.06	0.28
900	Air	1.43	0.82	2.25	0.57
700	N_2	1.39	0.81	2.20	0.58
800	N_2	1.11	1.04	2.15	0.93
900	N_2	1.13	1.05	2.18	0.93

3. Sensing characteristics

For the perovskite-type oxides the conductivity is due to the ionizing vacancies. The vacancies are formed in general in the following processes.

Ln Frenkel disorder: $La_{La}^{x} \rightarrow V_{La}''' + La_i^{***}$

Fe Frenkel disorder: $Fe_{Fe}^{x} \rightarrow V_{Fe}''' + Fe_i^{***}$

Oxygen Frenkel disorder: $O_O^{x} \rightarrow V_O'' + O_i^{**}$

$LnFeO_3$ full Schottky disorder: "nil" $\rightarrow V_{La}''' + V_{Fe}''' + 3V_o^{**} + LnFeO_3^{surf}$

Ln_2O_3 partial Schottky disorder: "nil" $\rightarrow 2V_{La}''' + 3V_O^{**} + Ln_2O_3^{surf}$

Fe_2O_3 partial Schottky disorder: "nil" $\rightarrow 2V_{Fe}''' + 3V_O^{**} + Fe_2O_3^{surf}$

The Frenkel disorders may be unfavorable. As indicated in **Table 1**, the coverage of Ln on the surface was higher than that of Fe. It seems that in the process of calcinations they lost the Ln atoms at the cranky points in the bulk and left the Ln vacancies. When the sensors exposed to O_2 and/or O_3, the oxygen was adsorbed on the surfaces, which would trap electron from the oxide due to the strong electro-negativity of the oxygen atom. So the concentration of holes in valence band increased. When organic compounds reacted with the adsorbed oxygen, the electron released from the adsorbed oxygen would annihilate the holes: $h + e \rightarrow 0$. Hence, the conductivity of the sensor decreased.

The sensitivity (conductance change) for NO_2 was influenced by Ln species of $LnFeO_3$. The correlation between the response (defined to the ratio $G_{10ppmNO2}/G_{air}$ of conductance in 10 ppm NO_2 and air) and the ratio of Ln/(Ln+Fe)

determined by the surface analysis is shown in **Fig.5**. Extremely larger response was confirmed for $SmFeO_3$. The higher response may be related to the higher coverage of NO_2.

Ozone and other oxidizing gases, such as NO_2, and Cl_2, are widely used in various technical processes and medicine. Ozone is applied in such fields as food, pharmaceutical, textile, and chemical industries, water treatment, purification of gases, and so on. Furthermore, the ozone is essential for life on the earth in its function as a protective layer against UV radiation and is present in concentrations of up to 8 ppm at a highest of approximately 30 km. On the other hand, ozone is one part of the summer smog and toxic. In the office environment, photocopiers and laser printers produce ozone. The legislations of most countries have established threshold values for long and short time exposure periods. Regarding with ozone, the environmental air quality is classified as follows: very good (0-50 ppb), Good (50-100ppb), Poor (100-200ppb), and Very Poor (>200ppb). The natural background-level is 30ppb. Therefore, it is very important to monitor the concentration of ozone in an atmosphere. The direct determination of ozone in the gas-phase in a higher ppb and ppm range is possible with sensors based on semiconducting oxide films such as In_2O_3 and WO_3. Both oxides are act as n-type semiconductor and the conductance decrease with an increase in the concentration of ozone in the atmosphere. The sensing characteristic of the $SmFeO_3$ based device was examined in lower concentration region below ca. 1ppm ozone. The conductance increased with an increase in the ozone concentration. The developed sensor exhibits a high sensitivity to ozone concentration of sub-ppm levels. The ozone molecule is catalytically decomposed on the metal oxides. The decomposition of ozone results the increase in the adsorbed oxygen acting the suprafacial active sites and in the partial pressure of oxygen of the ambient. It should be noted that, the catalytic activity is enhanced by the existence of

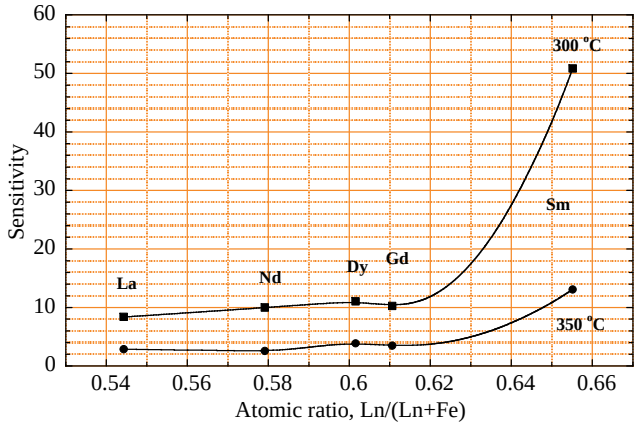

Fig. 5. Correlation between the rersponse to 10ppmNO_2 and Ln/(Ln+Fe) for $LnFeO_3$. Ln species and temperature were indicated in the figure.

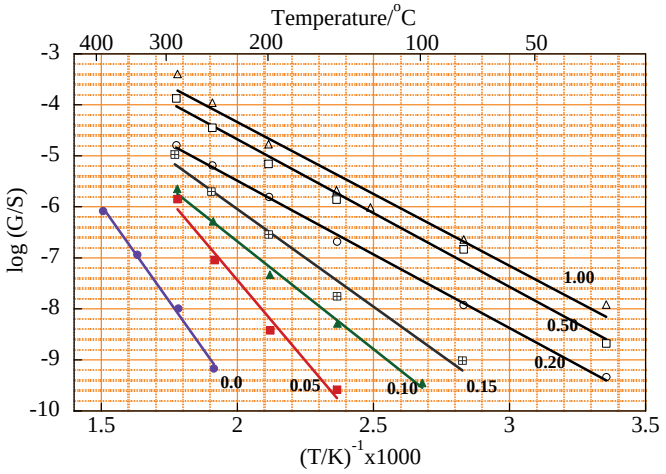

Fig. 6. Temperature dependence of the conductivity of the sensors in air. Co-content, x, is denoted in the figure.

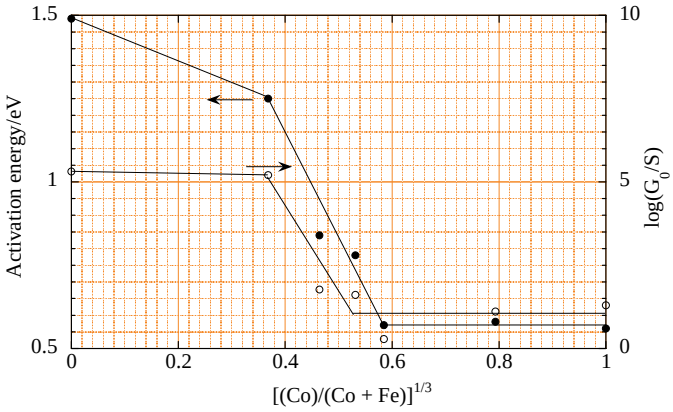

Fig. 7. Co-content dependence of the activation energy and G_0 in air.

ozone for Fe and Co-oxides, while CO_2 and H_2O are act as catalytic inhibiters.

The conductivity and the sensing characteristics of $SmFeO_3$ were influenced by the partial replacement of Fe with Co. **Figure 6** shows the temperature dependence of the conductivity in air of the $SmFe_{1-x}Co_xO_3$ based devices. The activation energy (E_a) evaluated from the plot was decreased with increase in the Co-content and for $x \geq 0.2$ it became nearly constant as shown in **Fig. 7**. The activation energy (E) and pre-exponential factor (G_0) were calculated by the Arrhenius relationship ($GT=G_0\exp(-E/kT)$, k=Boltzmann constant) using straight relationship in **Fig. 6**. The measurable value of conductivity was down to 10^{-10} S level by using the ultra high resistance meter with applied voltage of 0.10V. It seems that for $SmFeO_3$ the conductivity is also controlled by the hole production at Fe-sites, $Fe^x \rightarrow Fe' + Fe^*$, and with increasing the Co-content, double exchange effect between Co^{3+} and Co^{4+} is additionally contributed to the enhance of the bulk conductivity in air. For example, for x=0 the minimum operating temperature was 250°C, where the base conductivity is 6.80×10^{-10}S, but the minimum temperature was lowered with the Co-content. For $x \geq 0.20$, the reliable level's conductivity was obtained in air even at room temperature (**Fig.6**).

The conductivity measurements were carried out also in 0.4ppm O_3 and 10ppm NO_2. The results are shown in **Figs.8 and 9**, respectively. In both the circumstances, the conductivities of the devices were increased by the exposure of the oxidative gases. This increment of the conductivity indicates that the examined perovskite type oxides posses a p-type semiconducting feature. The temperature dependence of sensitivity is shown in **Figs.10 and 11**. In the case of ozone,

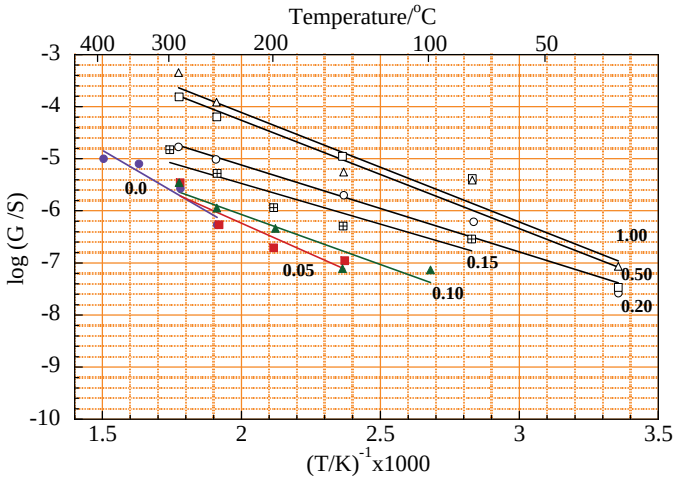

Fig. 8. Temperature dependence of the conductivity of the sensors in 0.4 ppm O_3. Co-content, x, is denoted in the figure.

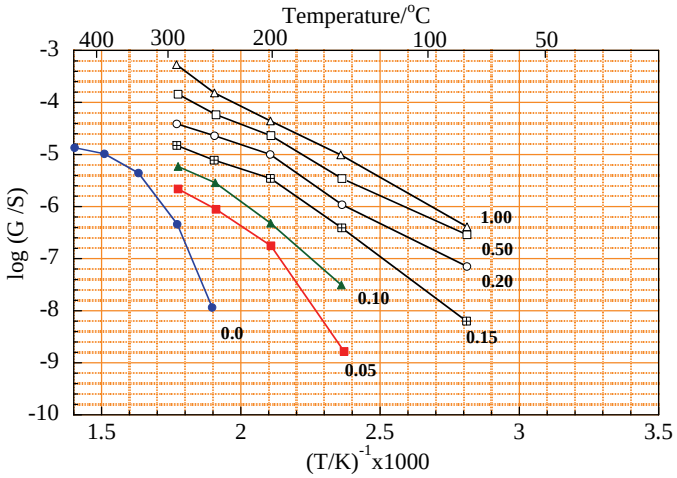

Fig. 9. Temperature dependence of the conductivity of the sensors in 10 ppm NO_2. Co-content, x, is denoted in the figure.

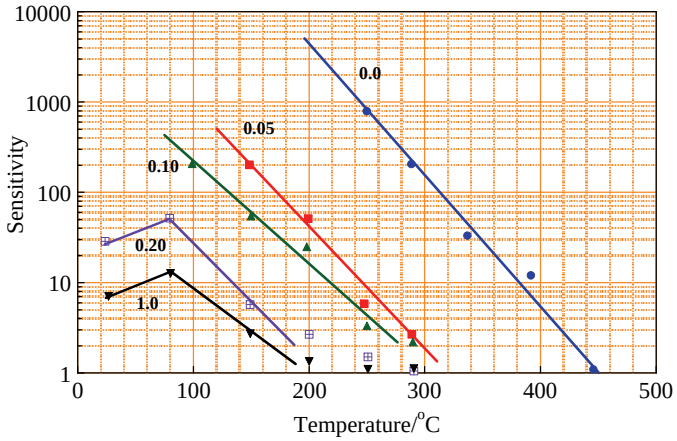

Fig.10. Response to 0.4 ppm ozone of the sensors at different temperatures. Co-content,x, is denoted in the figure.

the sensitivity, G(test gas)/G(air) was monotonically increased with a decrease in temperature, and decreased with an

increase in the Co-contents. For x=0.2, 0.5 and 1.0, their maximum responses were observed at 80°C but it was lower than 100. The response to NO_2 for the x=0.05-0.5 increased down to 200°C and decreased by further lowering temperature. For the x=0 and 1.0 the maximum response was observed at 290 and 150°C, respectively. Among of them, the device with x=0.05 showed the highest sensitivity, that was ca, 23. The sensitivity in NO_2 was much lower than that in O_3.

The conductance decreased by the contamination of MEK and EtOH as shown in **Fig.12,** while was hardly changed with same level of benzene for all examined devices. The highest response (S_{max}) for EtOH and MEK was observed at around 350°C for the device with $SmFeO_3$ and decreased with an increase in the temperature. The temperature of S_{max} decreased with an increase in Co-content of the device and the S_{max} also decreased. For VOCs, its electron donating behavior resulted the negative adsorption to the oxide resulting the decrease in the conductance. Additionally catalytic activity of the oxides should be considered. If VOCs were oxidized completely in catalytic, the final decomposed products are CO and H_2O, following CO and the chemisorbed oxygen O_{ad}^- can take place the reaction: $CO + O_{ad}^- \rightarrow CO_2 + e^-$. The decomposition of VOCs to CO resulted to the decrease in the conductance. It is known that perovskite materials act as an catalyst of oxidation of hydrocarbon and oxygenated compounds. The oxidation of toluene to benzaldehyde on $LaCoO_3$ in the temperature range of 350-600°C has been reported. [31]. The maximum of the catalytic activity observed at 500°C. It seems that the increase in the activity was ascribed to removal of surface contaminations and to the generation of structural defects such as anion vacancies. The activity decrease above 500°C was assumed to be due to a self-oxidations of the VOCs. Shimizu [32] found the oxides, $LaMO_3$(M=Mn, Fe, Co, Ni) to be active for oxidation of ethanol to acetaldehyde in the temperature range of

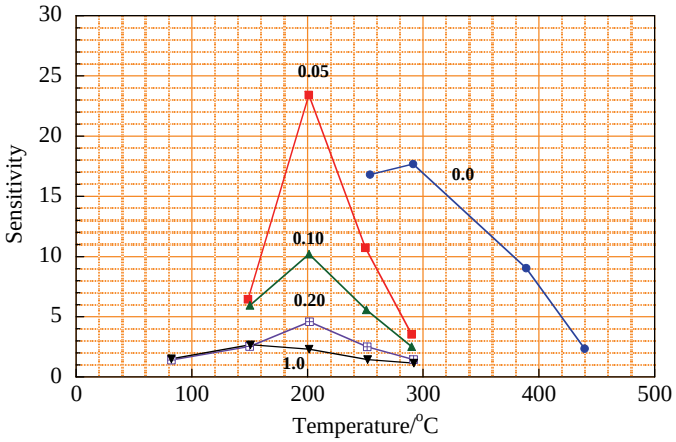

Fig.11. Response to 10 ppm NO_2 of the sensors at different temperatures. Co-content,x, is denoted in the figure.

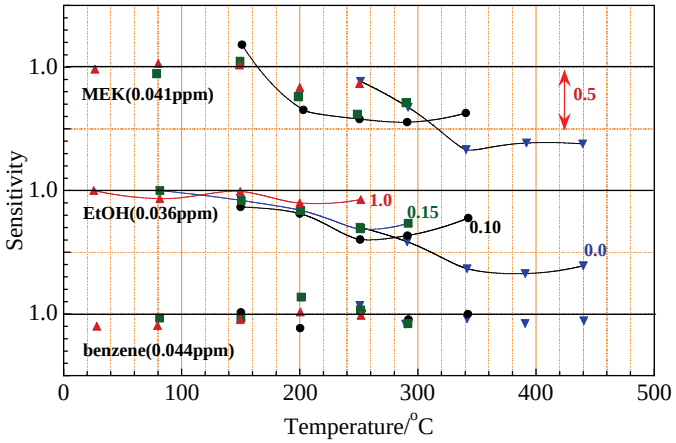

Fig. 12. Responce to VOCs of the sensors. Co-content,x, is indicated in the figure.

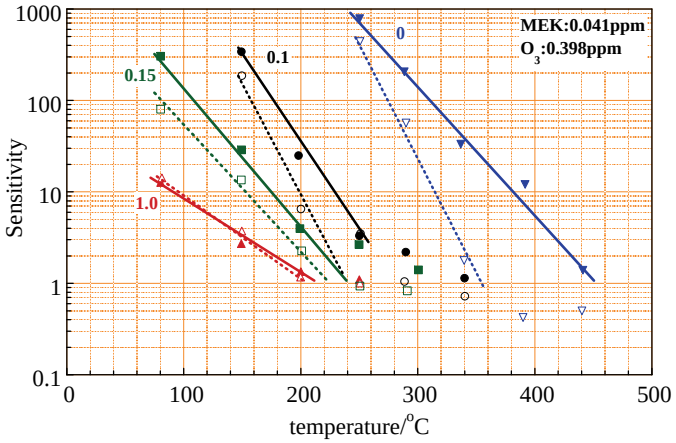

Fig.13. Response to O_3 with (broken) and without (solid) MEK of the sensors. Co-content,x, is indicated in the figure.

200-450°C. However, complete oxidation proceeded above 350°C and at higher O_2 partial pressure. The activity of $LaMO_3$ oxides decreased in the sequence Co>Mn>Ni>Fe. The clo se parallelism between oxygen adsorption and catalytic activity for total oxidation of propane and isobutene indicates that these reactions occur through a suprafacial catalysis mechanism in which adsorbed oxygen is the dominant species partic ipating in the reaction [33]. The homomolecular exchange of oxygen (HEO) on $LaMO_3$ (M=Cr, Mn, Fe, Co, Ni) and $LnCoO_3$ (Ln=Nd, Sm) oxides has been investigated in a broad range of temperatures [34]. The observed parallelism between the activation energies of the exchange of oxygen for the $LaMO_3$ compounds in the high-temperature region above 300°C and the energy of the oxygen bond (M-O) for the simple oxides of the transition elements suggest that the catalytic activity of the $LaMO_3$ oxides in the HEO is determined by the M^{3+} ions with no significa nt contribution of the La^{3+} ions in the compounds. However, the similarity of the temperature dependence of the exchange for $LnMO_3$ and the corresponding Ln_2O_3 (Ln=La, Nd. Sm) oxides in the low-temperature range below 200°C, suggested that the HEO is due to the Ln^{3+} cations. As mentioned above, Shimizu [32] found the oxides, $LaMO_3$(M=Mn, Fe, Co, Ni), to be active for oxidation of ethanol and complete oxidation proceeded above 350°C and at higher O_2 partial pressure. The activity of $LaMO_3$ oxides decreased in the sequence Co>Mn>Ni>Fe. As shown in **Fig.12**, the highest response (S_{max}) for EtOH was observed at around 350°C for the device with $SmFeO_3$ and decreased with an increase in the temperature. The temperature, T_{max}, at S_{max} decreased and the S_{max} decreased with an increase in the Co-content. The observed lower response at T_{max} for the device with a higher Co-content is not related to the catalytic activity differences between Fe- and Co- ions as reported. If VOCs molecule oxidized with adsorbed oxygen on the particles, the concentrations of adsorbed oxygen and the holes decreased. Also the replacing of adsorbed oxygen with electron donating VOCs and the interaction of VOCs with adsorbed oxygen result the decrease in the conductivity. It should be noticed that it seems that Co ion is act as an active site for the oxidation of VOCs and also effective to enhance the bulk conductivity by the exchange of 3d-electron between Co^{3+} and Co^{4+}. The enhancement of the bulk conductivity in air results the decrease in the response to VOCs.

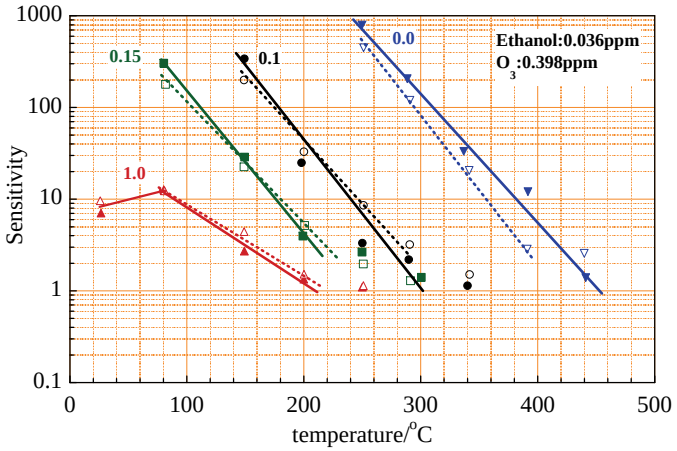

Fig. 14. Response to O_3 with (broken) and without (solid) EtOH of the sensors. Co-content,x, is indicated in the figure.

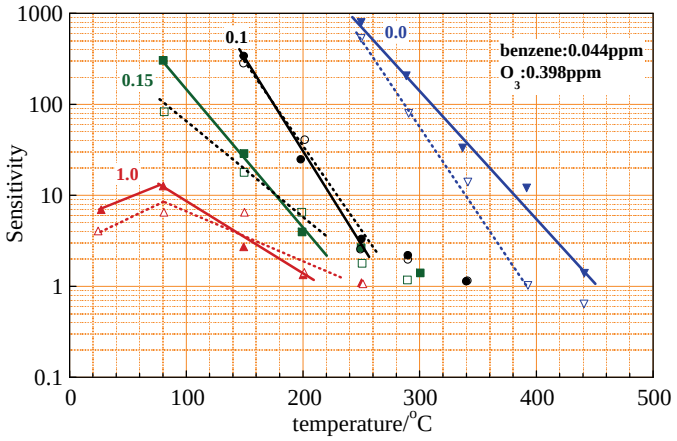

Fig. 15. Response to O_3 with (broken) and without (solid) benzene of the sensors. Co-content,x, is indicated in the figure.

Ozone is an oxidative agent (electron affinity; 2.1eV) and reactive with many kind of organic compounds. In gas-phase, several saturated hydrocarbons such as methane, ethane and hexane, are oxidized by ozone resulting the corresponding aldehyde, ketone, alcohol, and acid, while the oxidation process is in complex. In addition, catalytical behavior for the

oxidation is also observed for diluted ozone. The sensitivity to ozone may be strongly influenced by the contamination with VOCs. The effects of the contamination on the sensitivity to ozone were examined. The results for MEK, EtOH and benzene are shown in **Figs.13-15**. The lowering in the response to ozone was confirmed for these VOCs. To detect the ozone, the operation at a lower temperature is preferable to depress the effects of the contaminated VOCs.

4. Summary

Finer perovskite-type $LnFeO_3$ (Ln=La, Nd, Sm, Gd, and Dy) powders prepared by the pyrolysis of heteronuclear-complexes, $Ln[Fe(CN)_6]$ nH_2O. The thermal decomposition of CN-bridge induced the formation of perovskite-type oxide with the particle size of in the order of 20nm. With an increase in the temperature, the particle size increased from 20 nm (350°C) to 400nm (1000°C). For $SmFeO_3$ prepared by the decomposition of the complex at 900°C, the sensing characteristics were examined for ozone, NO_2, MEK, EtOH and benzene. The highest response was observed for ozone and estimated to 1000 for 0.1ppm at 250°C. The partial replacing Fe with Co resulted the enhancement of the conductivity in air with and without ozone. The enhancement of the conductivity made possible to decrease in the operation temperature of the sensor and the response of $SmFe_{0.90}Co_{0.10}$ O_3 was 50 and 3 for 0.4ppm ozone and 10ppmNO_2, respectively, at 150°C. Below 200°C, the conductivity was not responded to VOCs, such as MEK, EtOH and benzene. The developed sensors are very promising candidate for the detection of sub-ppm level's ozone. The lowering in the operation temperature of the sensor made possible to use a finer perovskite-type oxide for semiconductive gas sensor.

References

1. J.G.McCarty and H.Wise, *Catalysis Today*, **8**, 231 (1990).
2. N.Q.Minh, *J. Am. Ceram. Soc.,* **76**, 563 (1993).
3. T.Inoue, N. Seki, K.Eguchi, and H.Arai, *J. Electrochem. Soc.,* **137**, 2523 (1990).
4. P.Shuk, A Vecher, V.Kharton, L.Tichonova, H.D.Wiemhöfer, U.Guth, and W.Göpel, *Sensors and Actuators B*, **16**, 401 (1993).
5. T.Arakawa, H.Kurachi and J.Shiokawa, *J. Mater. Sci.,***4**, 1207 (1985).
6. Y.Shimizu, M.Shimabukuro, H.Arai, and T.Seiyama, *Chem. Lett.,* **1985**, 917.
7. T.Arakawa, K.Takada, Y.Tsunemine, and J.Shiokawa, *Sensors and Actuators,* **14**, 215(1988).
8. Y.Matsuura, S.Matsushima, M.Sakamoto, and Y.Sadaoka, *J. Mater. Chem.,* **3**, 767 (1993).
9. E.Traversa, S.Matsushima, G. Okada, Y.Sadaoka, Y.Sakai, K.Watanabe, *Sensors and Actuators B,* **24/25**, 600, (1995).
10. M. Kakihana, *J. Sol-Gel Sci. Technol.,* **6**, 7 (1996).
11. P.K. Gallagher, *Mat. Res. Bull,* **3**, 225 (1968).
12. F. Hulliger, M. Landolt, and H. Vetsch, *J. Solid State Chem.,* **18**, 283 (1976).
13. Y.Sadaoka, E.Traversa, and M.Sakamoto, *Chem.Lett.,* **1996**,177-178.
14. E.Traversa, M.Sakamoto and Y.Sadaoka, *J. Am. Ceram. Soc.,* **76**, 1401-1404 (1996).
15. Y. Sadaoka, E.Traversa and M. Sakamoto, *J. Alloys Compounds,* **240**, 51-59 (1996).
16. Y. Sadaoka, E.Traversa and M. Sakamoto, *J. Mater. Chem.,* **6**,1355-1360 (1996).
17. E.Traversa, P.Nunziante, G.Gusmano, M.Sakamoto, and Y. Sadaoka, *Mater. Sci. Forum,* **203**, 47-52(1996)
18. E.Traversa, P. Nunziante, M. Sakamoto, Y. Sadaoka, M.C. Carotta, and G.Martinelli, *J. Mater. Res.,* **13**(5), 1335-1344 (1998).
19. Y.Sadaoka, H.Aono, E.Traversa, M.Sakamoto, *J. Alloys and Compounds,* 278,135-141 (1998)
20. H.Aono, K.Kinoshita, M.Sakamoto, Y.Sadaoka, *J. Ceram. Soc. Jpn,* **106**(10), 958-963(1998)
21. G.Martinelli, M.C.Carotta, M.Ferroni, Y.Sadaoka, E.Traversa, *Sensors and Actuators*, B55, 99-110 (1999)
22. E.Traversa, S,Villanti, G.Gusmano, H.Aono, Y.Sadaoka, *J. Am. Ceram. Soc.,* **82**(9), 2442-2450(1999).

23. E.Traversa, P.Nuntiante, L.Sangaletti, B.Allieri, E.Depero, H.Aono, Y.Sadaoka, *J. Am. Ceram. Soc.,* **83**(5), 1087-1092 (2000).
24. E.Traversa, Y.Sadaoka, M.C.Carotta, G.Martinelli*, Sensors and Actuators,* **B 65**, 181-185(2000).
25. S.Matsushima, N.Sano, Y.Sadaoka, *J. Ceram. Soc. Jpn,* **108**(7), 681-682 (2000).
26. H.Aono, J.Ohmori, Y.Sadaoka, *J. Ceram. Soc. Jpn,* **108**(10), 892-897 (2000).
27. H.Aono, M.Sato, E.Traversa, M.Sakamoto, Y.Sadaoka*, J. Am. Ceram. Soc.,* **84**(2), 341-347 (2001).
28. H.Aono, M.Tsuzaki, A.Kawaura, M.Sakamoto, E.Traversa, Y.Sadaoka, *J. Am. Ceram. Soc.,* **84**(5), 969-975 (2001).
29. H.Aono, E.Traversa, M.Sakamoto, Y.Sadaoka*, Sensors and Actuators,* **B94** (7), 132-139(2003).
30. Y.Hosoya, Y.Itagaki, H.Aono, Y.Sadaoka, *Sensors and Actuators*, **B108**, 198-201 (2005).
31. Viswanathan,B., and George, S., Indian J*. Chem., Sect.*A 22A,1026(1983).
32. Shimizu.T., *Appl.Catal*., 28, 81(1986).
33. L. G. Tejuca, J. G.Fierro, and J.M.D.Tascon, *Advances in catalysis*, Vol.36. P-288.
34. L. G. Tejuca, J. G.Fierro, and J.M.D.Tascon, *Advances in catalysis*, Vol.36. P-305.